Accretion of Mudstone Beds from Migrating Floccule Ripples

Juergen Schieber, *et al.*

Science **318**, 1760 (2007);
DOI: 10.1126/science.1147001

Science (print ISSN 0036-8075; online ISSN 1095-9203) is published weekly, except the last week in December, by the American Association for the Advancement of Science, 1200 New York Avenue NW, Washington, DC 20005.

12. The sample could be transferred between the reactor and UHV chamber without exposure to air (*5*, *6*). The UHV chamber (base pressure ~ 1×10^{-10} torr) was equipped with instrumentation for XPS, low-energy electron diffraction, ion-scattering spectroscopy, and thermal-desorption mass spectroscopy.
13. S. Ma, X. Zhao, J. A. Rodriguez, J. Hrbek, *J. Phys. Chem. C* **111**, 3685 (2007).
14. X. Zhao, S. Ma, J. Hrbek, J. A. Rodriguez, *Surf. Sci.* **601**, 2445 (2007).
15. Z. Song, J. Hrbek, R. Osgood, *Nano Lett.* **5**, 1327 (2005).
16. F. Esch *et al.*, *Science* **309**, 752 (2005).
17. J. Nakamura, J. M. Campbell, C. T. Campbell, *J. Chem. Soc. Faraday Trans.* **86**, 2725 (1990).
18. C. V. Ovesen, P. Stoltze, J. K. Nørskov, C. T. Campbell, *J. Catal.* **134**, 445 (1992).
19. J. Zhou, D. R. Mullins, *Surf. Sci.* **600**, 1540 (2006).
20. C. T. Au, W. Hirsch, W. Hirschwald, *Surf. Sci.* **197**, 391 (1988).
21. O. Dulub *et al.*, *Science* **317**, 1052 (2007).
22. To estimate the TOF of CeO_{2-x}/Au(111) surfaces, we took into account the area covered by the oxide NPs and the concentration of O vacancies. It was assumed that all the atoms of a flat Cu(100) surface are active in the WGS reaction. This is a common assumption (*17*, *18*).
23. The unrestricted DF calculations were performed with the DMol3 code, treating molecules, nanostructures, and extended surfaces with the same level of accuracy (*11*, *24*). Au(100), Au(111), and TiO_2/Au(111) were modeled by means of the supercell approach with three-layer gold slabs and an 11 Å vacuum between the slabs (*11*). The top layer of the Au substrate, the oxide nanostructures, and the adsorbates were allowed to fully relax.
24. B. Delley, *J. Chem. Phys.* **92,** 508 (1990); **113,** 7756 (1992).
25. T. Albaret, F. Finocchi, C. Noguera, *Faraday Discuss.* **114**, 285 (1999).
26. V. A. Bondzie, S. C. Parker, C. T. Campbell, *Catal. Lett.* **63**, 143 (1999).
27. B. K. Min, C. M. Friend, *Chem. Rev.* **107**, 2709 (2007).
28. M. S. Chen, D. W. Goodman, *Science* **306**, 252 (2004).
29. N. C. Hernández, J. F. Sanz, J. A. Rodriguez, *J. Am. Chem. Soc.* **128**, 15600 (2006).
29. The work performed at Brookhaven National Laboratory was supported by the U.S. Department of Energy, Office of Basic Energy Sciences, under contract DE-AC02-98CH10886. J.E. and M.P. are grateful to Intevep for partial support of the work carried out at the Universidad Central de Venezuela.

4 September 2007; accepted 22 October 2007
10.1126/science.1150038

Accretion of Mudstone Beds from Migrating Floccule Ripples

Juergen Schieber,[1]* John Southard,[2] Kevin Thaisen[1]

Mudstones make up the majority of the geological record. However, it is difficult to reconstruct the complex processes of mud deposition in the laboratory, such as the clumping of particles into floccules. Using flume experiments, we have investigated the bedload transport and deposition of clay floccules and find that this occurs at flow velocities that transport and deposit sand. Deposition-prone floccules form over a wide range of experimental conditions, which suggests an underlying universal process. Floccule ripples develop into low-angle foresets and mud beds that appear laminated after postdepositional compaction, but the layers retain signs of floccule ripple bedding that would be detectable in the rock record. Because mudstones were long thought to record low-energy conditions of offshore and deeper water environments, our results call for reevaluation of published interpretations of ancient mudstone successions and derived paleoceanographic conditions.

A century ago, Henry Clifton Sorby, one of the pioneers of geology, pointed to the study of muds as one of the most challenging topics in sedimentary geology (*1*). Today, with our knowledge clearly expanded, muddy sediments are still considered highly complex systems that may require as many as 32 variables and parameters for a satisfactory physicochemical characterization (*2*). More research may clarify interdependencies between a number of these parameters and may allow us to consider a smaller number of variables, but the fundamental complexity of muddy sediments is likely to remain. A key issue in mudstone sedimentation is flocculation, a phenomenon in which a number of these parameters, such as settling velocity, floccule size, grain-size distribution, ion exchange behavior, and organic content "come together." A joining of smaller particles to form larger aggregates, flocculation enhances the deposition rate of fine-grained sediments, and its understanding is critical for modeling the behavior of mud in sedimentary environments.

Flocculation is affected by particle concentration within the fluid and intensity of turbulence (*3*, *4*). Over time, floccules enlarge to a maximum equilibrium diameter that is related to the intensity of turbulence (*5*). Floccule deposition is influenced by turbulence, bed shear stress, sediment concentration, and settling velocity. We currently still miss critical data on floccule formation and on the influence of floccule structure and turbulence on the formation of muddy sediments (*6*). We will collect data concerning these issues with new instrumentation in the near future, although the importance of our observations will not be affected. The notion is widely held that slow-moving currents or still water are a prerequisite for substantial mud deposition (*7*, *8*) because shear stress in swift-moving currents disrupts previously formed fragile floccules and prevents their deposition, but our observations suggest an alternative mode of mud deposition that apparently left its imprint in the rock record.

Mudstones constitute up to two-thirds of the sedimentary record and are arguably the most poorly understood type of sedimentary rocks (*9*). Mudstone successions contain a wealth of sedimentary features that provide information about depositional conditions and sedimentary history (*10*–*13*), but presently we lack the information that would allow us to link features observed in the rock record to measurable sets of physical variables in modern environments.

Although various small-scale sedimentary structures have been described from modern muds, these have not been observed in the making. This forces us to infer controlling parameters (e.g., current velocity and density of suspension) from temporally and spatially very limited measurements in the overlying water column (*14*–*17*). Such measurements (e.g., flow velocity, sediment concentration) in modern environments are commonly considered representative of depositional conditions for the uppermost millimeters to decimeters of the accumulating deposits. However, upon close examination, modern sediments show considerable heterogeneity at the millimeter to centimeter scale (*16*), an indication that what we observe in surficial sediments is not a direct response to measured conditions in the overlying water column. To improve on this situation, it is essential to conduct experiments that replicate natural conditions and to compare the experimental sediments to the rock record.

Here, we report experimental insights into the sedimentology of mudstones. In past experimental studies, centrifugal pumps were used to recirculate mud suspensions (*18*–*20*), destroying the clay floccules that are of such key importance in mud transport and deposition. Therefore, to minimize the risk of shredding clay floccules once formed, we built a racetrack flume that uses a paddle belt (*21*) for moving the mud suspension.

The racetrack flume (fig. S1) used for these experiments (*21*) has a 25-cm-wide channel. The effective flow depth was 5 cm. Powdered kaolinite clay (Fig. 1A) was mixed with water and added into the flume, running at 50 cm/s velocity (*21*). Sediment concentrations ranging from 0.03 g/l to 2 g/l were explored, and suspended sediment concentrations were monitored with an optical turbidity sensor. Experiments were conducted in distilled water, fresh (tap) water, and salt water (35 per mil salinity). In a few experiments, Ca-montmorillonite and natural lake mud (sieved to 63 μm) was used.

Addition of clay to the flume resulted within minutes in the formation of "floccule streamers" that mark boundary-layer streaks (*22*). Floccules range in size from 0.1 mm to almost 1 mm (Fig. 1, B to D) and were sampled and examined with a scanning electron microscope (SEM). After establishment of a stable suspended clay concentration, the velocity was stepwise reduced (Fig. 2) until the critical velocity of sedimentation was reached (*23*). At that point, a linear decline of sediment concen-

[1]Department of Geological Sciences, Indiana University, Bloomington, IN 47405, USA. [2]Department of Earth and Planetary Sciences, Massachusetts Institute of Technology, Cambridge, MA 02139, USA.

*To whom correspondence should be addressed. E-mail: jschiebe@indiana.edu

tration was observed and essentially all sediment settled out of the flow (Fig. 2). By shining strong lights from above through the flow, we were able to photograph and film floccule streamers (Fig. 3A), individual migrating floccules, floccule ripples (Fig. 3B), and fields of floccule ripples (Fig. 3C).

Floccules that give rise to "floccule streamers" (Fig. 3A) form even at small sediment concentrations (0.03 g/l), in both distilled water and fresh water, and increase in abundance as velocity is lowered. Below the critical velocity of sedimentation (Fig. 2), patches of floccules form and organize into streamlined ripples that migrate slowly downcurrent (Fig. 3, B to D). The critical velocity for sedimentation depends on initial sediment concentrations and ranges from ~10 cm/s for small sediment concentrations (0.03 g/l) to at least 26 cm/s for sediment concentrations in the 1 to 2 g/l range. In several experiments where flow was stopped suddenly and water was drained and replaced with clear water, floccules were observed on the foreset slopes of floccule ripples (Fig. 3E).

We also conducted experiments in which we introduced multiple sediment pulses and allowed the clay to accumulate at the bottom before adding the next pulse (*21*). A small amount of pulverized hematite (a red powder) was added between clay pulses to mark the tops of successive clay pulses. This addition of clay increments and hematite spikes was repeated until a sediment layer of approximately 2 cm (uncompacted thickness) had accumulated. At the end of the flume run, draining of the water typically revealed that the mud bed carried at its surface elongated ripples that stood up to 3 cm above the flume bottom and were spaced between 30 and 40 cm apart in the downstream direction (Fig. 3D and fig. S2). These experimental mud layers were air-dried to the consistency of soft butter and scraped with a butter knife or spatula to reveal internal layering outlined by hematite drapes. These internal layers were inclined in the downcurrent direction (fig. S3), indicating lateral accretion of clays. Once the clay beds have dried completely, these internal laminae appear to layer parallel on surfaces perpendicular to bedding (Fig. 4A). Drying out, however, also leads to separation of the top portions of layers along bottom-parallel fractures and reveals that the overall deposit is characterized by low-angle, downcurrent-dipping cross-strata (Fig. 4B).

These observations show that ripples composed of clay floccules migrated over the flume bottom at the onset of deposition (Fig. 3) and that a rippled bed topography was present at the end of deposition (fig. S2). In addition, the texture produced by the low-angle, downcurrent-dipping cross-strata in Fig. 4B has a direct textural analog in sandstones, where it is known as "rib and furrow" structure (*24*). The latter is seen on horizontal surfaces cut through sandstone beds that accumulated from migrating ripples. Closer inspection of the surface exposed in Fig. 4B shows the deposits of multiple overriding floccule ripples (fig. S4). Under the microscope, the inclined clay laminae from Fig. 4B show a "bumpy" surface pattern of closely packed ovoid bodies (0.2 to 0.6 mm in size) (fig. S5), the compacted floccules from which the migrating ripples and the accreting clay bed were constructed.

It appears that irrespective of what drives flocculation in a given experiment, flocculation provides deposition-prone particles without fail over a wide range of experimental conditions. Formation of floccule ripples from a variety of clay-size materials (kaolinite, montmorillonite, and lake mud), and over a range of sediment concentrations and salinities (distilled, fresh, and salt water) strongly suggests a universal process at work.

Our observations do not support the notion that muds can only be deposited in quiet environments with only intermittent weak currents (*8*). Instead, bedload transport of flocculated mud and deposition occurs at current velocities that would also transport and deposit sand (*21*). Clay beds can accrete from migrating floccule ripples under swiftly moving currents in the 10 cm/s to 26 cm/s velocity range, a range likely to expand as flows with larger sediment concentrations are explored. Whereas the clay beds formed in our experiments consist of downcurrent-inclined laminae, they appear to be parallel-laminated once fully compacted (Fig. 4A). Because floccule ripples are spaced 30 to 40 cm apart, ancient sediments of this origin are likely to appear parallel-laminated (Fig. 4C) as well. Detection of ripple-accreted muds in the rock record will require carefully defined, and yet to be developed, criteria. Things to look for might be subtle nonparallel lamina geometry, as well as basal downlap and top truncation of laminae. Examination of ancient shale units may, for example, yield low-amplitude bedforms (Fig. 4, D and E) as indicators of lateral accretion and ripple migration. Bedding-oblique orientation of larger flat particles, such as spores, microfossils, plant debris, and mica flakes, could be another indicator. If such particles are deposited on the inclined foresets of floccule ripples, they may record the gentle inclination of the latter even when compaction has rendered the depositional fabric of inclined laminae (Fig. 4B) unrecognizable.

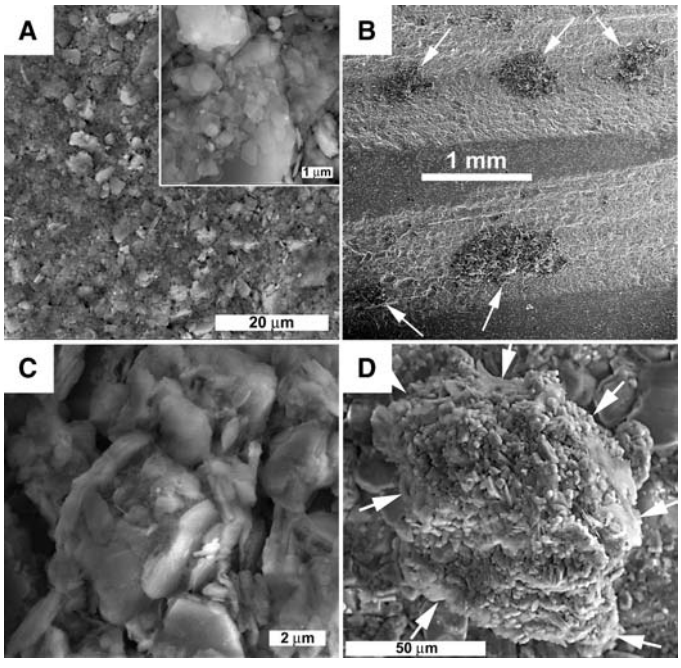

Fig. 1. Flume feed and floccules. (**A**) SEM image of typical kaolinite clay used in the majority of experiments. Inset shows size and morphology of clay flakes. (**B**) SEM image of floccules (pointed out by arrows) that were trapped at the flume bottom with a grooved glass slide. (**C**) Close-up of floccules in (B). (**D**) SEM image of a floccule (outline marked with white arrows). This floccule measures 0.12 mm along the long axis.

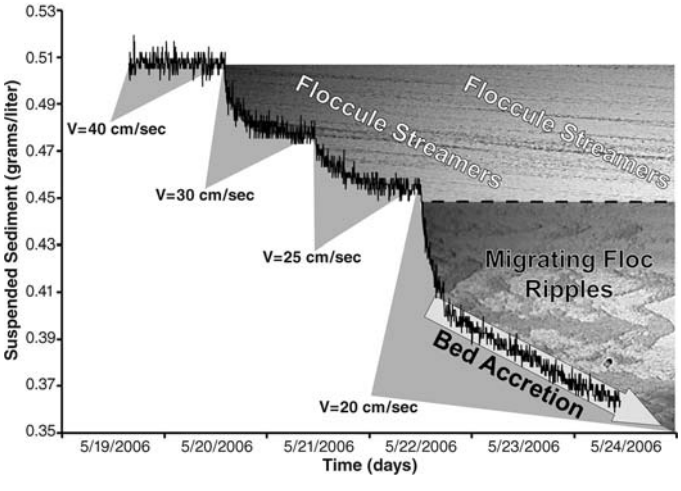

Fig. 2. Example of changes in suspended sediment in the course of an experiment. Vertical axis shows continuously logged suspended sediment concentration, and horizontal axis shows time elapsed (tick marks separate successive days). The critical velocity of sedimentation lies between 25 cm/s and 20 cm/s and coincides with the onset of development of floccule ripples. Its exact determination requires the use of smaller velocity steps.

In the course of two decades of detailed studies of shales and mudstones, one of us (*25*–*27*) has seen comparable low-amplitude bedforms (Fig. 4D) in shale units that were deposited in a wide variety of environments. Examples can be found in the Mid-Proterozoic Belt Supergroup, the Devonian of the eastern United States, the Jurassic Posidonia Shale, the Cretaceous Mancos Shale, and the Eocene Green River Formation. This suggests that mud accretion from migrating floccule ripples probably occurred throughout geologic history. Many ancient shale units, once examined carefully, may thus reveal that they accumulated in the manner illustrated here, rather than having largely settled from slow-moving or still suspensions. This, in turn, will most likely necessitate the reevaluation of the sedimentary history of large portions of the geologic record.

Elucidating the mechanisms of mudstone deposition not only helps to better understand the rock record but also benefits hydrocarbon exploration, hydrogeology, and coastal and shelf engineering. Managing mud is important for the maintenance of harbors, shipping lanes, and water reservoirs, especially given the impact of climate change. How mudstones act as barriers to fluid migration (oil and water) is probably linked to depositional processes that affect mud microfabrics. For example, if a mud accumulated from current-transported floccules, one might expect a network of larger pores, poorer sealing capacity, and easier release of liquid and gaseous hydrocarbons. Conversely, accumulation in still water from dispersed clays and low-density floccules should lower permeability and may produce an oil shale that clings tightly to its generated hydrocarbons. These qualities are also critical for the ability of a mudstone unit to protect aquifers from contamination and to compartmentalize groundwater reservoirs.

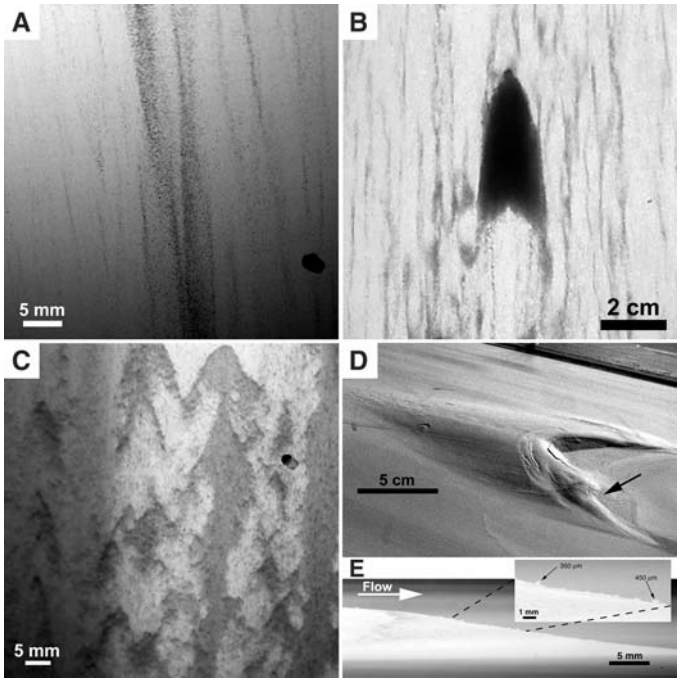

Fig. 3. (**A**) Floccule streamers photographed through the flume bottom (flow velocity 48 cm/s, initial sediment concentration 0.72 g/liter, lake mud in tap water). (**B**) Streamlined floccule ripple and floccule streamers. (**C**) Multiple floccule ripples begin to coalesce. Flow is from top to bottom in images (A), (B), and (C). (**D**) Oblique view of large barchan-shaped migrating floccule ripple. Flow is toward the right. (**E**) Side view of the left horn of this ripple [pointed out by black arrow in (D)]. Inset shows that the surface is covered with small, round bodies, the clay floccules that moved across the ripple during current activity. Numbers indicate floccule size.

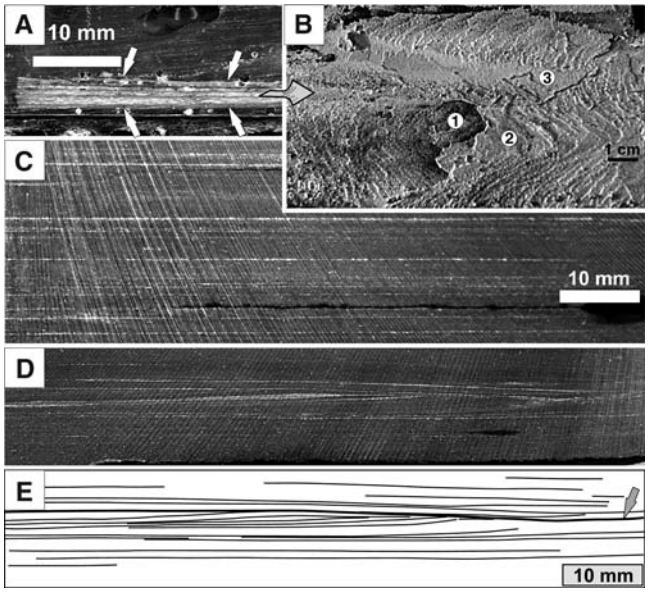

Fig. 4. (**A**) Laminated flume sediment (between white arrows) that was deposited during an experiment with continuous current flow. Sample was embedded in epoxy and cut perpendicular to bedding. Sample is curved due to desiccation. The darker internal laminae are hematite markers. (**B**) Textural detail from the interior of the clay layer in (A) (top view, arrow indicates 90° twist). As the layer dried out, its upper portion formed concave desiccation polygons, whereas its lower portion remained attached to the flume bottom. Removing the upper portion exposes a bottom-parallel surface through the clay layer. The curved lines are the upper terminations of broken foreset laminae of floccule ripples. The foreset laminae are inclined to the right, and the circled numbers indicate a succession of overriding ripples (see also fig. S4). The overall texture resembles "rib and furrow" structures as known from current rippled sandstones (*24*). (**C**) Parallel-laminated black shale, New Albany Shale, Devonian, Indiana. Lighter laminae are silt-enriched. (**D**) Cross-laminated shale collected from the same core box as (C). (**E**) Tracing of silt laminae visible in (D). Arrow marks an internal erosion surface. In the center are inclined (to the left) truncated laminae, forming the outline of a compacted and mud-dominated ripple. The synoptic relief of this ripple is 3 mm, but its original relief would have been ~20 mm (assuming 85% water content), the same magnitude as observed in our experiments.

References and Notes

1. H. C. Sorby, *Q. Geol. Soc. London* **64**, 171 (1908).
2. J. Berlamont, M. Ockenden, E. Toorman, J. Winterwerp, *Coast. Eng.* **21**, 105 (1993).
3. H. A. Einstein, R. B. Krone, *Proc. J. Hydr. Div.* **H12**, 51 (1961).
4. I. N. McCave, in *Fine-Grained Sediments: Deep Sea Processes and Facies*, D. A. V. Stow, D. J. W. Piper, Eds. (Geological Society of London, London, 1984), pp. 35–69.
5. E. Parthenaides, *Proc. J. Hydraulics Div.* **91**, 105 (1965).
6. J. C. Winterwerp, C. Kranenburg, *Fine Sediment Dynamics in the Marine Environment, Proceedings in Marine Science 5* (Elsevier, Amsterdam, 2002).
7. P. E. Potter, J. B. Maynard, W. A. Pryor, *Sedimentology of Shale* (Springer Verlag, New York, 1980).
8. P. E. Potter, J. B. Maynard, P. J. Depetris, *Mud and Mudstones: Introduction and Overview* (Springer, New York, 2005).
9. J. Schieber, in *Shales and Mudstones (vol. 1): Basin Studies, Sedimentology and Paleontology*, J. Schieber, W. Zimmerle, P. Sethi, Eds. (Schweizerbart'sche Verlagsbuchhandlung, Stuttgart, 1998), pp. 131–146.
10. N. R. O'Brien, R. M. Slatt, *Argillaceous Rock Atlas* (Springer Verlag, New York, 1990).
11. J. Schieber, *Sedimentology* **33**, 521 (1986).
12. J. Schieber, *Sedimentology* **36**, 203 (1989).
13. J. Schieber, in *Shales and Mudstones (vol. 1): Basin Studies, Sedimentology and Paleontology*, J. Schieber, W. Zimmerle, P. Sethi, Eds. (Schweizerbart'sche Verlagsbuchhandlung, Stuttgart, 1998), pp. 187–215.
14. S. A. Kuehl, C. A. Nittrouer, D. J. DeMaster, *Cont. Shelf Res.* **6**, 311 (1986).
15. S. A. Kuehl, C. A. Nittrouer, D. J. DeMaster, *J. Sediment. Petrol.* **58**, 12 (1988).
16. S. A. Kuehl, T. M. Hariu, M. W. Sanford, C. A. Nittrouer, D. J. DeMaster, in *Microstructure of Fine-Grained Sediments*, R. H. Bennett, W. R. Bryant, M. H. Hulbert, Eds. (Springer Verlag, New York, 1991), pp. 33–45.
17. M. P. Segall, S. A. Kuehl, *Sediment. Geol.* **93**, 165 (1994).
18. N. Hawley, *Sedimentology* **28**, 699 (1981).
19. K. W. Pasierbiewicz, J. Kotlarczyk, *J. Sediment. Res.* **67**, 510 (1997).
20. J. H. Baas, J. L. Best, *J. Sediment. Res. Sect. A* **72**, 336 (2002).
21. Materials and methods are available as supporting material on *Science* Online.
22. J. R. L. Allen, *Principles of Physical Sedimentology* (George Allen and Unwin, London, 1985).

23. J. Berlamont, M. Ockenden, E. Toorman, J. Winterwerp, *Coast. Eng.* **21**, 105 (1993).
24. W. L. Stokes, *Primary Sedimentary Trend Indicators as Applied to Ore Finding in the Carrizo Mountains, Arizona and New Mexico, Part 1* (U.S. Atomic Energy Commission, Oak Ridge, TN, 1953).
25. J. Schieber, *Sedimentology* **36**, 203 (1989).
26. J. Schieber, in *Shales and Mudstones (vol. 1): Basin Studies, Sedimentology and Paleontology*, J. Schieber, W. Zimmerle, P. Sethi, Eds. (Schweizerbart'sche Verlagsbuchhandlung, Stuttgart, 1998), pp. 187–215.
27. J. Schieber, *J. Sediment. Res.* **69**, 909 (1999).
28. This research was supported by NSF grants EAR-0318769 and EAR-0617128.

Supporting Online Material
www.sciencemag.org/cgi/content/full/318/5857/1760/DC1
Materials and Methods
Figs. S1 to S5

25 June 2007; accepted 30 October 2007
10.1126/science.1147001

A Madden-Julian Oscillation Event Realistically Simulated by a Global Cloud-Resolving Model

Hiroaki Miura,[1]* Masaki Satoh,[1,2] Tomoe Nasuno,[1] Akira T. Noda,[1] Kazuyoshi Oouchi[1]

A Madden-Julian Oscillation (MJO) is a massive weather event consisting of deep convection coupled with atmospheric circulation, moving slowly eastward over the Indian and Pacific Oceans. Despite its enormous influence on many weather and climate systems worldwide, it has proven very difficult to simulate an MJO because of assumptions about cumulus clouds in global meteorological models. Using a model that allows direct coupling of the atmospheric circulation and clouds, we successfully simulated the slow eastward migration of an MJO event. Topography, the zonal sea surface temperature gradient, and interplay between eastward- and westward-propagating signals controlled the timing of the eastward transition of the convective center. Our results demonstrate the potential making of month-long MJO predictions when global cloud-resolving models with realistic initial conditions are used.

A Madden-Julian Oscillation (MJO) is an envelope of active convection thousands of kilometers wide that travels eastward at an average speed of 5 m/s over the Indian and Pacific Oceans (*1*). Given the large-scale (10^3 to 10^4 km horizontally) coupling between the atmospheric circulation and deep convection, an MJO influences not only the intraseasonal (30 to 90 days) variability of the tropics but also tropical cyclone genesis, the onset and break of the Asian-Australian monsoon, and the evolution of the El Niño–Southern Oscillation event (*2*, *3*). Despite its extensive effects on weather events and climate variability, weather prediction and climate models do not simulate the MJO well (*4*). Even recently, most of the coupled atmosphere-ocean general circulation models (GCMs) presented in the Fourth Assessment Report of the Intergovernmental Panel on Climate Change had difficulty simulating the variance and phase speed of the MJO (*5*). It is expected that weather forecasts beyond 10 days could be improved if the MJO representations in global weather prediction models were more realistic (*2*).

The major difficulty in simulating the MJO with GCMs involves cumulus parameterization used to estimate the vertical redistribution of heat and moisture by unresolved convective clouds in GCMs (*4*, *6*). Computational constraints have made it almost impossible to run global cloud-resolving models (GCRMs) that compute the effects of clouds explicitly and do not depend on cumulus parameterizations. However, recent increases in available computer power have begun to eliminate the models' artificial gap between cloud processes and the atmospheric circulation (*7*). Improved MJO simulations with GCMs substituting two-dimensional cloud-resolving models for cumulus parameterizations (*8*, *9*) suggest the importance of representing the variation in quasi-equilibrium states (*10*); that is, the statistical balance between stabilization by convection and destabilization by external forcing, which depends on large-scale atmospheric circulation. Therefore, GCRMs may allow realistic MJO simulations because convective activity can be linked directly to dynamic and thermodynamic atmospheric conditions of large-scale atmospheric circulation and convection. Here we report a numerical simulation of an MJO event that occurred between December 2006 and January 2007.

On the Earth Simulator, we ran a GCRM called the Nonhydrostatic Icosahedral Atmosphere Model (*11*), which has been upgraded as a result of aquaplanet experiments (*12*, *13*) and a realistic tropical cyclone experiment (*14*), with horizontal grids with mesh sizes about 3.5 and 7 km. These resolutions are almost fine enough to resolve the gross behavior of cumulus ensembles, including heating and moistening, as a response to large-scale atmospheric conditions. The 3.5-km grid run covered 1 week, whereas the 7-km grid run covered 30 days, which was long enough to reproduce the eastward migration of the convective center from the Indian to the Pacific Ocean. The initial atmospheric conditions were generated by linear interpolation from the National Centers for Environmental Prediction (NCEP) Global Tropospheric Analyses at 00:00 universal time coordinated (UTC) on 25 December 2006 for the 3.5-km grid run and at 00:00 UTC on 15 December 2006 for the 7-km grid run. We did not use any artificial techniques to nudge the model atmosphere to realistic atmospheric states during the numerical integrations (*15*).

The large-scale convectively active region of the MJO was reproduced approximately by the 3.5-km (Fig. 1) and 7-km (not shown in Fig. 1) grid runs. The convective center was near Borneo on 31 December 2006, and upper tropospheric clouds covered the islands of Southeast Asia and the surrounding seas. The typical multiscale structure of

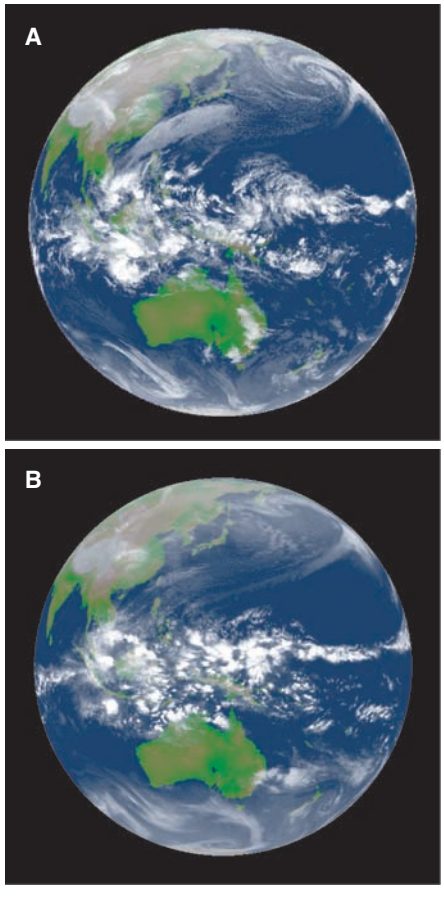

Fig. 1. (**A**) Infrared image from the Multi-Functional Transport Satellite (MTSAT-1R) at 00:30 UTC on 31 December 2006 and (**B**) outgoing longwave radiation from the 3.5-km run averaged from 00:00 UTC to 01:30 UTC on 31 December 2006.

[1]Frontier Research Center for Global Change, Japan Agency for Marine-Earth Science and Technology, 3173-25 Showamachi, Kanazawa-ku, Yokohama, Kanagawa 236-0001, Japan. [2]Center for Climate System Research, University of Tokyo, 5-1-5 Kashiwanoha, Kashiwa, Chiba 277-8568, Japan.

*To whom correspondence should be addressed. E-mail: miurah@jamstec.go.jp